NUKLEONIKA 2015;60(3):399–403
doi: 10.1515/nuka-2015-0071

ORIGINAL PAPER

DE GRUYTER
OPEN

EMR study and superposition model analysis of Cr^{3+} and Fe^{3+} impurity ions in mullite powders used in aerospace industry

Ireneusz Stefaniuk, Iwona Rogalska

Abstract. In this work, the electron magnetic resonance (EMR) spectra of the mullites powders were measured for different grain sizes (0.07 and 0.12 mm). We have used EMR spectroscopy at X-band, combined with superposition model (SPM) calculations to reveal electronic structure and establish correlations between structure, and surroundings of these complexes.

Key words: electron magnetic resonance (EMR) • mullites • spin Hamiltonian (SH) • superposition model (SPM)

Introduction

In this work, the electron magnetic resonance (EMR) spectra of the mullites powders were measured for different grain sizes (0.07 and 0.12 mm). We have used EMR spectroscopy at X-band, combined with superposition model (SPM) calculations to reveal electronic structure and establish correlations between structure, and surroundings of these complexes. The main purpose of this work was to investigate the possible relationships between EMR spectra and the size of powder grains, as well as the identification of EMR spectra in view of the potential application of EMR technique as a fingerprinting method [1, 2]. The motivation for this study comes from the need to solve the problem of fractures of shape and ceramic cores.

Mullite is the only stable intermediate phase in the alumina-silica system at atmospheric pressure. The chemical formula for mullite is deceptively simple: $3Al_2O_3{\cdot}2SiO_2$. However, the phase stability, crystallography, and stoichiometry of this material remain controversial. The structural variants are derived from the average structure considering crystal-chemical rules for bond lengths, atomic distances, and coordination number (Fig. 1) [3].

Considering these rules and different occupations of the Oc and Oc* sites, 34 structural variants result from the decomposition of the mullite average structure. Each four variants exhibit an oxygen vacancy on the same cell edge and different occupations of the Oc and Oc* sites on the remaining three edges. Structural variants 17 to 32 are vacancy free, but with a variation on the Oc/Oc* sites. Variants 33 and 34 represent the silica free i-Al_2O_3 modification [3].

I. Stefaniuk✉, I. Rogalska
Faculty of Mathematics and Natural Sciences,
University of Rzeszow,
1 Pigonia Str., 35-959 Rzeszow, Poland,
Tel.: +48 17 851 8672,
E-mail: istef@ur.edu.pl

Received: 1 October 2014
Accepted: 30 January 2015

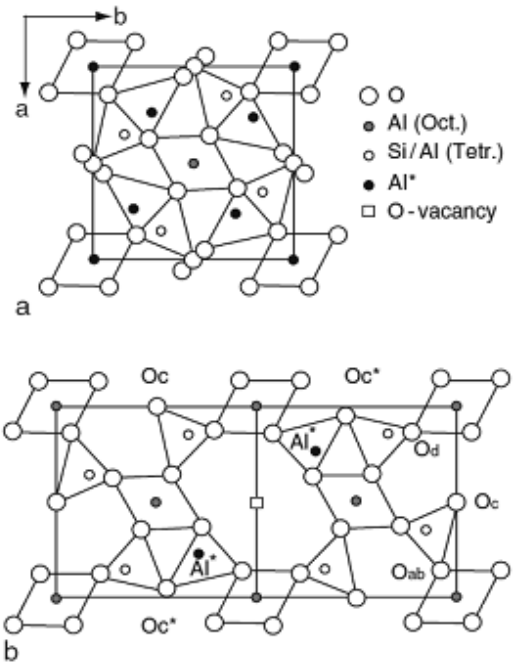

Fig. 1. Structure of mullite: (a) average structure and, (b) atomic displacements around an oxygen vacancy [3].

The occupation of the tetrahedral Si/Al and Al* sites depends on the position of oxygen atoms or vacancies. If the Oc site is occupied, the two adjacent Si/Al sites are occupied too. However, next to a vacancy, the adjacent Al* sites are occupied instead of the Si/Al sites, and the coordinating oxygen atoms shift from the Oc to the Oc* position (Fig. 1). Structural variants with two vacancies building the correlation vector <110> are not allowed, because an Al or Si atom would only be threefold coordinated. Si/Al-Oe* bond lengths of 0.173 and 0.178 nm lead to a tetrahedral occupation by Al, whereas 0.167 nm for the Si/Al-Oc bond gives Si occupation of the T position. EMR studies by Rager *et al*. [4] and us [1, 2] provided further information on the structural distribution of chromium in mullite. Chromium-doped mullites exhibit two rather sharp EMR signals near $g_{\text{eff}} = 5$, and a broad signal near $g_{\text{eff}} = 2.2$. The peaks near $g_{\text{eff}} = 5$ were assigned to Cr^{3+} in slightly distorted octahedral M(1) positions in mullite, whereas the broad slightly asymmetric signal near $g_{\text{eff}} = 2.2$ may indicate coupling between localized magnetic moments. Rager *et al*. [4] explained the signal at $g_{\text{eff}} = 2.2$ in terms of interstitial Cr^{3+} incorporation in mullite. According to the EMR peak intensities, the entry of Cr^{3+} into the regular M(1)O6 octahedra is favored at low bulk-Cr_2O_3 contents of mullite, whereas interstitial incorporation with formation of chromium clusters becomes more important at higher Cr_2O_3 contents [3, 4].

Experimental details

The EMR spectra of the mullites powders were measured for different grain sizes 0.07 mm (Al_2O_3 – 76.86%; SiO_2 – 22.8%) and 0.12 mm (Al_2O_3 – 75.04%; SiO_2 – 24.5%).

The EMR spectra were investigated in a wide range of temperatures from 120 to 380 K using an EPR X-band spectrometer (Bruker multifrequency and multiresonance FT-EPR ELEXSYS E580). Crystallographic data for mullite are: $a = 7.5785(6)$ Å, $b = 7.6817(7)$ Å, $c = 2.8864(3)$ Å, space group: *Pbam*, whereas structural parameters are listed in Table 1 [3, 4].

Spin Hamiltonian and SPM analysis of EMR spectra

Analysis of EMR spectra was performed using spin Hamiltonian (SH) suitable for transition ions [5]. For arbitrary low (triclinic) symmetry, SH [6, 7] is best expressed in terms of the extended Stevens operators (ESO) O_k^q [8, 9]:

$$(1) \qquad H_s = \mu_B B \cdot g \cdot S + \sum B_k^q O_k^q(S_X, S_Y, S_Z) = \mu_B B \cdot g \cdot S + \sum f_k b_k^q O_k^q$$

where g represents the Zeeman electronic tensor, B is the external magnetic field, S_i are the spin operators, and B_k^q (b_k^q) are the zero-field splitting parameters (ZFSPs). The 'scaling' factors f_k in Eq. (1) are most commonly defined as [6, 7]: $f_2 = 1/3$; $f_4 = 1/60$; $f_6 = 1/1260$. For proper relations between the conventional ZFSPs and B_k^q (b_k^q) in Eq. (1), see [6, 7, 10]. For Cr^{3+} ($S = 3/2$) ions only the ZFSPs with $k = 2$ are required, whereas for Fe^{3+} ($S = 5/2$) ions with $k = 2$ and 4.

For spin $S = 5/2$, the ZFS Hamiltonian in Eq. (1) includes the following terms for given symmetry cases: (1) tetragonal type II (groups: C_4, S_4, C_{4h}), for $k = 2$: $q = 0$; $k = 4$: $q = 0, 4, -4$; (2) orthorhombic (groups: D_2, C_{2v}, D_{2h}), for $k = 2$: $q = 0, 2$; $k = 4$: $q = 0, 2, 4$; (3) monoclinic (groups: C_2, $C_{1h}(C_s)$, C_{2h}) – assuming the monoclinic C_2 axis is parallel to the z axis, for $k = 2$: $q = 0, 2, -2$; $k = 4$: $q = 0, 2, -2, 4, -4$. Two other equivalent forms of monoclinic ZFS Hamiltonian should be considered if the magnetic axis x or y is chosen as parallel to the monoclinic C_2 axis [11]. For triclinic symmetry, all q components are included in Eq. (1). This paper is preliminary, whereas distinction between the actual low symmetry aspects and the apparent ones will be discussed in a full article.

Table. 1. Structural parameters for mullite (occupancy – occ.)

	Al	T	T*	Oab	Oc	Oc*	Od
x	0.0	0.14901(2)	0.26247(9)	0.3590(1)	0.5	0.4498(4)	0.1273(1)
y	0.0	0.34026(2)	0.20529(9)	0.4218(1)	0.0	0.0505(4)	0.2186(1)
z	0.0	0.5	0.5	0.5	0.5	0.5	0.0
occ.	1.0	0.56(2) Al 0.25(2) Si	0.13(2) Al 0.06(2) Si	1.0	0.39(1)	0.190(1)	1.0

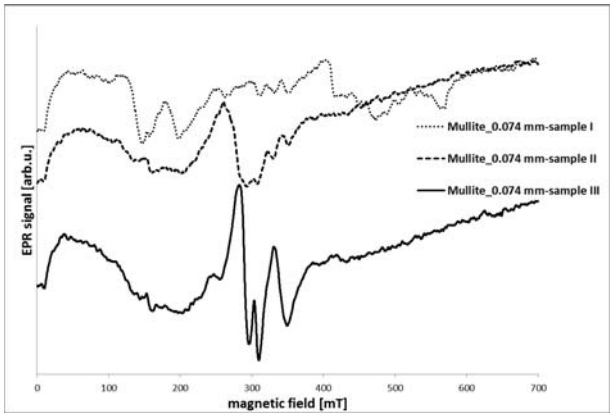

Fig. 2. EMR spectra in X-band for mullites samples from different part of materials commercially available with the same grain sizes.

Results and discussion

The selected obtained EMR spectra are presented in Fig. 2. Despite the similar chemical compositions of materials, differences between EMR spectra were detected.

The analysis of the line positions suggests that the lines with $g_{eff} = 4.28$ and $g_{eff} \approx 2.00$ may be attributed to Fe^{3+} ($S = 5/2$) ions, because they present a typical spectrum for so-called disordered systems [12] that present a glassy host [13]. The line intensities decrease progressively showing the evolution of the relative line shapes and the intensities at $g_{eff} = 4.3$ from isolated ions in local tetrahedral (and eventually octahedral) sites [13]. The line with $g_{eff} = 1.98$ may be attributed to Cr^{3+} ($S = 3/2$) ions in the slightly distorted octahedral sites [14].

In this paper, we present an extension of the computer program superposition model-Monte Carlo (SPM-MC) designed for modeling of the spectroscopic and structural properties of transition ions at low symmetry sites in crystals. This program is based on the SPM and the MC method [15–18], and uses the crystallographic and EMR data.

The first capability of the program SPM-MC is prediction of the structure of MLn complexes around paramagnetic transition ions at low symmetry sites in crystals, that is, the 'feasible ligands' positions distorted by an impurity. This is achieved by fitting the theoretical estimates to the experimental ZFSPs obtained from EMR spectra. The second capability is estimation of the ZFSPs based on the structural data and a suitable choice of the SPM parameters, that is, the intrinsic parameters: $\bar{b}_k(R_0)$, power-law exponents: t_k.

$$(2)\ \bar{b}_2(R) = (-A + B)\left(\frac{R_0}{R}\right)^{t_2} = A\left(\frac{R_0}{R}\right)^{n} + B\left(\frac{R_0}{R}\right)^{m}\ [\mathrm{cm}^{-1}]$$

with $\bar{b}_2(R_0) = (-A + B)$ in [cm^{-1}] and $m > n > 0$ [17].

Using SPM and crystallographic data, ZFSPs b_2^q and b_4^q are calculated for Cr^{3+} and Fe^{3+} ions at the Al_2O_3 and Cr_2O_3-site (with local tetrahedral and octahedral sites) [17–20]. Our SPM analysis of ZFSPs indicates that satisfactory agreement can be achieved between the theoretical and experimental results. Additional structural information about Cr^{3+} and Fe^{3+} impurity centers is also obtained.

For Cr^{3+} ions, which replace Al^{3+} in Al_2O_3, the constants A, B, n, m, t_k, (Eq. (1)) and the reference distance R_0 depend on the kind of impurity ions and their valence (definition in [15, 16, 21]) were obtained from the data in [22], and the crystallographic data from [4].

For illustration, we adopt the following values: $R_0 = 0.195$ nm, $n = 10$, $m = 13$, $A = -10.6$ cm^{-1}, and $B = -8.2$ cm^{-1}. Using the ZFSPs and the pertinent conversion relations provided in [10, 21], the program SPM-MC [15, 16] computes the feasible positions of the oxygen ligands in a given unit cell volume that yield the SPM-predicted ZFSPs consistent with the experimental ZFSPs.

Figure 3 presents the occupation of the octahedral sites (Oc*), whereas Fig. 4 shows the tetrahedral sites (T*). The numerical calculations and analysis were carried out for the complex $Cr(Al)O_6$ in Al_2O_3. These values were used to construct the $Cr(Al)O_6$ octahedron in Al_2O_3. ZFSPs b_2^q and b_4^q are calculated for Cr^{3+} and Fe^{3+} ions at the mullite with local tetrahedral and octahedral sites (see Table 2) from crystallographic data for T*, Oc* sites (see Fig. 1 and Table 1).

The SPM-calculated ZFSPs in Table 2 appear to be highly nonstandard. Standardization of orthorhombic and monoclinic ZFS (as well as crystal field) parameters [23, 24] will be considered in a full paper. Preliminary results for the impurity Cr^{3+} and

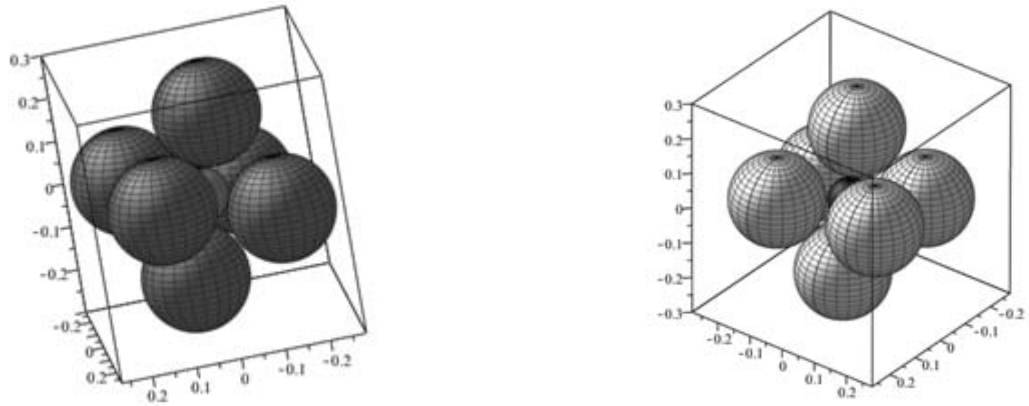

Fig. 3. The selected $Cr(Al)O_6$ (left) and $Fe(Al)O_6$ (right) octahedral for the obtained data.

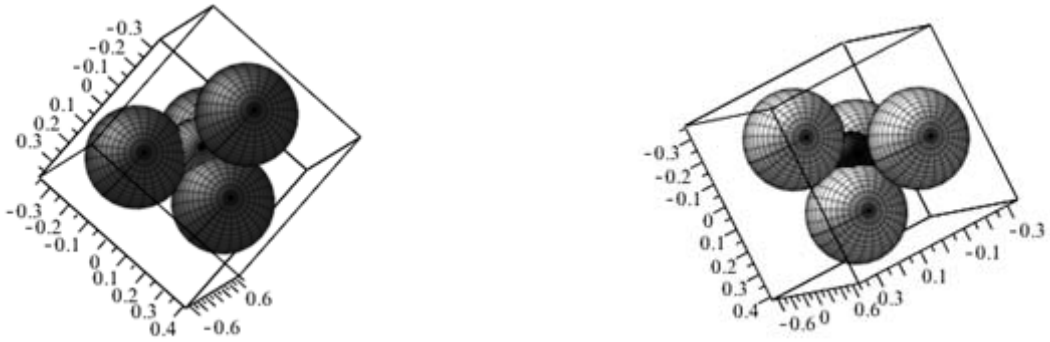

Fig. 4. The selected $Cr(Al)O_4$ (left) and $Fe(Al)O_4$ (right) tetrahedral for the obtained data.

Table 2. Monoclinic ZFSPs b_k^q calculated by SPM for Cr^{3+} and Fe^{3+} ions

	b_2^0	b_2^2	b_2^{-2}	b_4^0	b_4^2	b_4^4	b_4^{-2}	b_4^{-4}
$Cr^{3+}(6)$	–54.367	153.324	–217.399	–	–	–	–	–
$Fe^{3+}(6)$	–32.149	91.170	–129.310	–19.728	380.357	–246.955	–654.973	–463.511
$Cr^{3+}(4)$	111.797	102.943	94.906	–	–	–	–	–
$Fe^{3+}(4)$	66.588	61.560	55.943	12.474	364.335	–151.282	–104.429	–343.352

Fe^{3+} ions in mullite are presented. SPM analysis confirms the most probable model of distortions around Cr^{3+} and Fe^{3+} ions occupying the Al positions.

Figure 2 presents different concentrations of Cr^{3+} and Fe^{3+} ions in different occupations. Due to correlation between cracking ceramic forms and materials from various suppliers, it may be assumed that direct cause is distortion sizes related to occupation Cr^{3+} and Fe^{3+} ions. We are still working to confirm this correlation, details will be given elsewhere.

Calculations using SPM program were made based on structural data (see [3, 4]), which are related with the crystallographic axes (x, y, z).

Correlation of spectroscopic properties of Cr^{3+} with structural data in aluminosilicates were performed in [25, 26] based on calculations for the local occupations of Cr^{3+} ions for monoclinic (C_2, C_s, C_{2h}) and triclinic (C_1, C_i) symmetry. Our calculations, which are based on the works [25, 26] (see also [27]), use directly the crystallographic data for two different occupations: octahedral and tetrahedral, without the assumed symmetry (complete lack of symmetry), in the axis system compatible with crystallographic data [3, 4].

The main goal of this work is to demonstrate, based on the identified EPR lines, the correlation between EMR spectra of mullites and the distortions around the Cr^{3+} and Fe^{3+} ions calculated by the SPM program. From the information obtained from industrial facilities within the framework of the project "Modern material technologies in aerospace industry". We conclude that changes in the compositions of the starting materials act as a multiple source of cracking. We still carry out detailed investigation of the direct link between the observed spectra and mechanical properties of ceramic forms and cores.

Our calculations indicate the expected difference between the predicted ZFSPs of Cr^{3+} and Fe^{3+} ions. The second order SPM parameters: $R_0 = 0.195$ nm, $n = 10, m = 13, A = -10.6$ cm^{-1}, and $B = -8.2$ cm^{-1} employed in calculations were used for octahedral occupations in many work, e.g., [15, 16, 22]. The rank four SPM parameters were obtained with the unchanged second-order ones as: intrinsic parameter b_4^- [cm^{-1}] and power-law exponent $t_4 = 8.6$, which is dimensionless. This work confirms correlation between the ZFSPs obtained from experimental EMR spectra and structural data.

Conclusions

Using SPM and crystallographic data, the ZFS parameters b_2^q and b_4^q are calculated for Cr^{3+} and Fe^{3+} ions at the Al_2O_3 and Cr_2O_3 site (with local tetrahedral and octahedral sites). SPM analysis confirms the most probable model of distortions around Cr^{3+} and Fe^{3+} ions occupying the Al positions. The EMR spectra for these samples differ considerably concerning the shape, the intensity of individual components of the line, the width and the resolution, and the signal-to-noise ratio, even though they were obtained using the same spectrometer EPR during the same conditions. The predicted ZFSPs obtained based on SPM confirm correlation between the ZFSPs obtained from experimental EMR spectra and structural data. Detailed investigations are still carried out to confirm the direct link between the obtained spectra and mechanical properties of ceramic forms and cores.

Acknowledgments. Financial support of Structural Funds in the Operational Programme – Innovative Economy (IEOP) financed from the European Regional Development Fund – Project "Modern material technologies in aerospace industry", no. POIG.01.01.02-00-015/08-00 is gratefully acknowledged.

References

1. Stefaniuk, I., Potera, P., & Cebulski, J. (2010). The EPR measurements of Al_2O_3 powders and mullites

used in aerospace industry for cores and shapes. *Curr. Top. Biophys.*, *33*(Suppl. A), 227–230.
2. Stefaniuk, I., Rogalska, I., Potera, P., & Wróbel, D. (2013). EPR measurements of ceramic cores used in the aircraft industry. *Nukleonika*, *58*(3), 391–395.
3. Schneider, H., & Komarneni, S. (2006). *Mullite*. John Wiley & Sons. Retrieved 25 April 2006, from http://onlinelibrary.wiley.com/book/10.1002/3527607358. DOI: 10.1002/3527607358.
4. Rager, H., Schneider, H., & Graetsch, H. (1990). Chromium incorporation in mullite. *Am. Miner.*, *75*, 392–397.
5. Abragam, A., & Bleaney, B. (1986). *Electron paramagnetic resonance of transition ions*. New York: Dover.
6. Rudowicz, C. (1987). Concept of spin Hamiltonian, forms of zero-field splitting and electronic Zeeman Hamiltonians and relations between parameters used in EPR. A critical review. *Magn. Reson. Rev., 13*, 1–89; (1988) Erratum, *ibidem 13*, 335.
7. Rudowicz, C., & Misra, S. K. (2001). Spin-Hamiltonian formalisms in electron magnetic resonance (EMR) and related spectroscopies. *Appl. Spectrosc. Rev*., *36*, 11–63.
8. Rudowicz, C. (1985). Transformation relations for the conventional O_k^q and normalized $O'_k{}^q$ Stevens operator equivalents with $k = 1$ to 6 and $-k \le q \le +k$. *J. Phys. C*, *18*, 1415–1430; (1985) Erratum: *ibidem C*, *18*, 3837.
9. Rudowicz, C., & Chung, C. Y. (2004). The generalization of the extended Stevens operators to higher ranks and spins, and a systematic review of the tables of the tensor operators and their matrix elements. *J. Phys.-Condens. Matter*, *16*, 5825–5847.
10. Rudowicz, C. (2000). On the relations between the zero-field splitting parameters in the extended Stevens operator notation and the conventional ones used in EMR for orthorhombic and lower symmetry. *J. Phys.-Condens. Matter*, *12*, L417–L423.
11. Rudowicz, C. (1986). On standardization and algebraic symmetry of the ligand field Hamiltonian for rare earth ions at monoclinic symmetry sites. *J. Chem. Phys*., *84*, 5045–5058.
12. Griscom, D. L. (1980). Electron spin resonance in glasses. *J. Non-Cryst. Solids*, *40*, 211–272.
13. Berger, R., Yahiaoui, E. M., Bissey, J. -C., Béiade, P., Kliava, J., Zinsou, P. K., & Beziade, P. (1995). Diluted and non-diluted ferric ions in borate glasses studied by electron paramagnetic resonance. *J. Non-Cryst. Solids, 180*, 151–163.
14. Simion, S., van der Pol, A., Reijerse, E. J., Kentgens, A. M., van Moorsel, G. J., & de Boer, E. (1995). Magnetic resonance studies on porous alumina doped with iron and chromium. *J. Chem. Soc. Faraday Trans*., *91*(10), 1519–1522.
15. Stefaniuk, I., & Rudowicz, C. (2010). Computer program SPM-MC and its applications in EMR studies of transition ions in crystals. *Curr. Top. Biophys., 33*(Suppl. A), 217–220.
Stefaniuk, I., & Rudowicz, C. (2013). Computer program superposition model-Monte Carlo (SPM--MC) and its applications in EMR studies of transition ions at low symmetry sites Fe^{3+} doped YAP crystals. *Nukleonika*, *58*(3), 397–400.
16. Newman, D. J., & Urban, W. (1975). Interpretation of S-state ion E.P.R. spectra. *Adv. Phys., 24*, 793–844.
17. Newman, D. J., & Ng, B. (1989). The superposition model of crystal fields. *Rep. Prog. Phys., 52*, 699–763.
18. Rudowicz, C. (1987). On the derivation of the superposition-model formulae using the transformation relations for the Stevens operators. *J. Phys. C-Solid State Phys., 20*, 6033–6037.
19. Yeom, T. H., Chang, Y. M., Choh, S. H., & Rudowicz, C. (1994). Experimental and theoretical investigations of spin Hamiltonian parameters for the low symmetry Fe^{3+} centre in $LiNbO_3$. *Phys. Status Solidi B-Basic Solid State Phys.*, *52*, 409–415.
20. Stefaniuk, I., Rudowicz, C., Gnutek, P., & Suchocki, A. (2009). EPR study of Cr^{3+} and Fe^{3+} impurity ions in nominally pure and Co^{2+}-doped $YAlO_3$ single crystals. *Appl. Magn. Reson., 36*, 371–380.
21. Müller, K. A., & Berlinger, W. (1983). Superposition model for sixfold-coordinated Cr^{3+} in oxide crystals. *J. Phys. C-Solid State Phys*., *16*, 6861–6874.
22. Rudowicz, C., & Bramley, R. (1985). On standardization of the spin Hamiltonian and the ligand field Hamiltonian for orthorhombic symmetry. *J. Chem. Phys*., *83*, 5192–5197.
23. Kripal, R., Yadav, D., Gnutek, P., & Rudowicz, C. (2009). Alternative zero-field splitting (ZFS) parameter sets and standardization for Mn2+ ions in various hosts exhibiting orthorhombic site symmetry. *J. Phys. Chem. Solids*, *70*, 827–833.
24. Qin, J., Rudowicz, C., Chang, Y. M., & Yeung, Y. Y. (1994). Correlation of spectroscopic properties and substitutional sites of Cr^{3+} in aluminosilicates: II. Andalusite and sillimanite. *Phys. Chem. Miner., 21*, 532–538.
25. Yeung, Y. Y., Qin, J., Chang, Y. M., & Rudowicz, C. (1994). Correlation of spectroscopic properties and substitutional sites of Cr^{3+} in aluminosilicates: I. Kyanite. *Phys. Chem. Miner., 21*, 526–531.
26. Yeung, Y. Y. (2013). Superposition model and its applications. In M. G. Brik & N. M. Avram (Eds.), *Optical properties of 3d-ions in crystals: Spectroscopy and crystal field analysis* (Chapter 3). Springer and Tsinghua University Press.